Beach-ridge architecture constrained by beach topography and ground-penetrating radar, Itilleq (Laksebugt), south-west Disko, Greenland – implications for sea-level reconstructions

PRISCILA E. SOUZA, AART KROON & LARS NIELSEN

Souza, P.E., Kroon, A. & Nielsen, L. 2018. Beach-ridge architecture constrained by beach topography and ground-penetrating radar, Itilleq (Laksebugt), south-west Disko, Greenland – implications for sea-level reconstructions. © 2018 by Bulletin of the Geological Society of Denmark, Vol. 66, pp. 167–179. ISSN 2245-7070. (www.2dgf.dk/publikationer/bulletin). https://doi.org/10.37570/bgsd-2018-66-08

Received 24 November 2017
Accepted in revised form
19 April 2018
Published online
7 September 2018

Detailed topographic data and high-resolution ground-penetrating radar (GPR) reflection data are presented from the present-day beach and across successive raised beach ridges at Itilleq, south-west Disko, West Greenland. In the western part of the study area, the present low-tide level is well defined by an abrupt change in sediment grain size between the sandy foreshore and the upper shoreface that is characterised by frequently occurring large clasts. The main parts of both fine and large clasts appear to be locally derived. Seaward-dipping reflections form downlap points, which are clearly identified in all beach-ridge GPR profiles. Most of them are located at the boundary between a unit with reflection characteristics representing palaeo-foreshore deposits and a deeper and more complex radar unit characterised by diffractions; the deeper unit is not penetrated to large depths by the GPR signals. Based on observations of the active shoreface regime, large clasts are interpreted to give rise to scattering observed near the top of the deeper radar unit. We regard the downlap points located at this radar boundary as markers of palaeo-low-tide levels. In some places, scattering hyperbolas are more pronounced and frequent than in others, suggesting differences in the occurrence of large boulders.

Keywords: Downlap points, sea level, berm evolution, beach ridges, Arctic coasts.

Priscila E. Souza [pes@ign.ku.dk], Aart Kroon [ak@ign.ku.dk], Lars Nielsen [ln@ign.ku.dk], Department of Geosciences and Natural Resource Management, Faculty of Science, University of Copenhagen, Øster Voldgade 10, DK-1350 Copenhagen, Denmark.

Corresponding author: Priscila E. Souza.

After the deglaciation of the coastal area of Disko between 9.25 ka and 9 ka before present, the sea transgressed to the Holocene marine limit (Ingólfsson *et al.* 1990). The elevation of marine limits increased from *c.* 50 m to *c.* 90 m in a south-east direction across Disko, indicating that the western areas experienced lower rates of land rise than the eastern ones (Ingólfsson *et al.* 1990). Marine terraces and successive beach ridges were formed below the marine limit during the emergence of coasts (Donner 1978; Rasch & Nielsen 1995).

Most beach ridges are relict berms. They originate in the intertidal and supratidal zones by wave-related processes, mainly swash, backwash and percolation, and are preserved as the shoreline progrades (Otvos 2000). Understanding how berms are formed and evolve in time and space on the current active beach is a helpful tool to assess and interpret the internal structure of beach ridges and to point out reliable past sea-level markers (Bendixen *et al.* 2013). Moreover, beach-ridge deposits have been used as sea-level indicators in numerous studies in temperate as well as Arctic and Antarctic coastal regions (Rodriguez & Meyer 2006; Nielsen & Clemmensen 2009; Simms *et al.* 2011; Pedersen *et al.* 2011; Lindhorst & Shutter 2014; Billy *et al.* 2015; Nielsen *et al.* 2017). However, their present surface morphology in Artic regions may not accurately correspond to past sea level, because of subsequent surface erosion, solifluction processes and/or sediment redeposition (e.g. Nielsen *et al.* 2017). Such processes may have altered the surface significantly.

On the other hand, the internal structure of beach ridges is often well preserved and can be depicted from ground-penetrating radar (GPR) data. The GPR reflections, which are observations in the recorded data, reveal the bed morphology and thus constitute a potentially important key for reconstruction of past sea levels as seen from GPR investigations at different localities (Tamura *et al.* 2008; Nielsen & Clemmensen 2009; Clemmensen & Nielsen 2010; Hede *et al.* 2013), including Disko and southern Greenland (Nielsen *et al.* 2017).

Nielsen *et al.* (2017) document characteristics of numerous fossil raised beach ridges from the south-east coast of Disko and two localities in South Greenland. They identified several downlap points in the internal structure of these fossil ridges. Downlap points were interpreted to represent levels correlated to sea level at the time of deposition, most likely close to low-tide levels. The specific depth with respect to sea level is dependent on factors such as local wave conditions and tidal ranges.

In this paper, we document the internal architecture of modern and fossil beach ridges at Itilleq (Laksebugt), south-west Disko. We use observations of well-developed modern analogues to constrain our interpretation of the fossil, raised systems. We identify several downlap points in the internal sedimentary structure of fossil raised beach ridges at Itilleq. The downlap points are interpreted in relation to past sea level at the time of deposition and a model for berm formation with respect to the sea level at the time of deposition is presented. This model is based on investigation of a well-developed modern analogue in the area. Our work provides a basis for later reconstruction of a detailed relative sea-level (RSL) curve for Itilleq, provided that the past sea-level markers are dated.

Study area

Itilleq is an embayment on the south-western coast of Disko, central West Greenland (Fig. 1). Disko is mainly covered by Tertiary plateau basalts (Pedersen *et al.* 2000), but sedimentary deposits characterise the

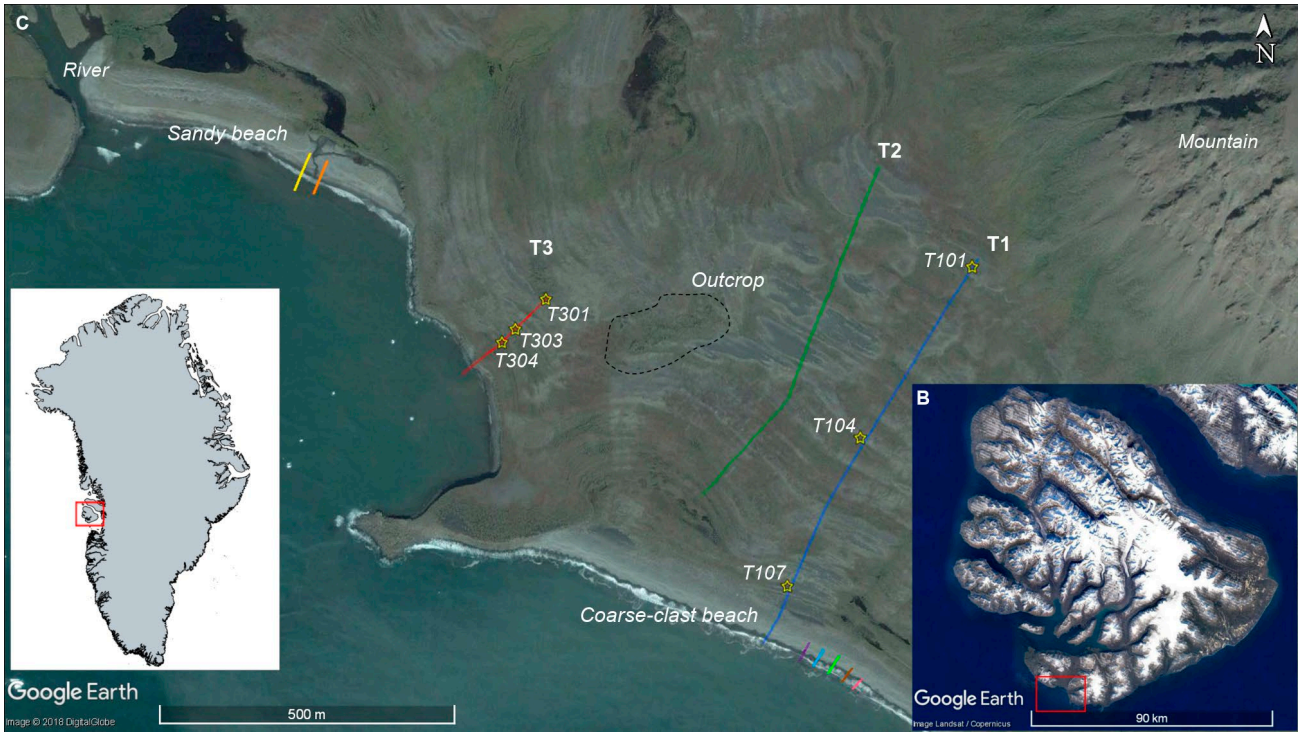

Fig. 1. Study area. **A**: Overview map of Greenland showing the location of Disko island on the west coast (red box). **B**: Satellite image of Disko showing the location of Itilleq (red box). **C**: Satellite image of Itilleq showing the location of both sandy and coarse-clast present-day beaches. Coloured lines: GPR transect lines. Yellow stars: the location and code of holes dug along the transects. The local sediment sources are river, outcrop and mountain. Differently coloured GPR transects across recent beaches represent: Line 26 (purple), Line 27 (blue), Line 28 (green), Line 29 (brown) and Line 30 (pink) on the coarse-clast beach, and Line 32 (orange) and Line 33 (yellow) on the sandy beach. The three GPR transects across beach ridges are labelled T1 to T3. Satellite images in B and C are generated by Google Earth (provided, respectively, by Landsat/Copernicus in December 2016, and by DigitalGlobe on August 23, 2004).

Itilleq coastal area, where relatively wide stretches of beach deposits as well as coastal cliffs occur. Alluvial fans and a marine terrace extend from the base of the steep mountain slopes, more than 40 m above the lowest astronomical tide, down to either the present shoreline or to the top of coastal cliffs located about 8 m above the lowest astronomical tide.

Successive beach ridges are present on the lower slopes of the talus of the mountains and the marine terrace. They are mainly NW–SE oriented but change orientation at their western end, becoming N–S oriented (Fig. 1C). The beach ridges are mainly covered by lichen-covered, round boulders. Swales between the ridges are also characterised by coarse-grained material but more remarkably by an uneven hummocky terrain, 'patterned ground', a characteristic feature generated by freezing and thawing processes (French 1996).

Two beaches occur in the area: a western, sandy beach and an eastern, coarse-clast beach with a mixture of sand and gravel. The shorelines of both beach types are aligned nearly NW–SE but differ in their exposure to incoming waves. The beach types are separated by a cuspate foreland which projects from the western end of the coarse-clast beach and therefore shields the sandy beach from wind waves coming from the east (Fig. 1C).

The sandy beach is approximately 500 m long; it is cut by a river at its northern end and bordered by the N–S oriented coastal cliff at the cuspate foreland at its southern end (Fig. 1C). The western half of this beach is up to 100 m wide. Here, there is a clear berm with a gradually dipping backshore ending in a lagoon. The eastern half of the sandy beach is narrower (10 to 60 m wide) and steeper. Its easternmost part is backed by an 8 m high cliff that separates the present-day beach system from the inland alluvial fans and marine terraces. The coarse-clast beach is twice as long as the sandy beach and not separated by any cliffs from the marine terrace. Towards the east, the shoreline orientation turns to N–S and is interrupted by a river (not shown in Fig. 1C). Cobble- and boulder-size sediments prevail all over the beach stretch.

The climate in the area is polar maritime with an annual mean temperature of -4° C (Ingólfsson *et al.* 1990). Easterly winds are the most frequent all year around (Fig. 2). However, they do not contribute significantly to wave generation because Itilleq is an embayment on the coast facing south-west (Fig. 1B), sheltered at its east side by land. An ice-free period generally occurs from late May to November (Danish Meteorological Institute, DMI 2015). The coastal area experiences a semidiurnal meso-tidal regime. The average tidal range is 1.34 m at Qeqertarsuaq town 15 km east of Itilleq, with maximum spring tidal levels of 2.5 m above mean low water.

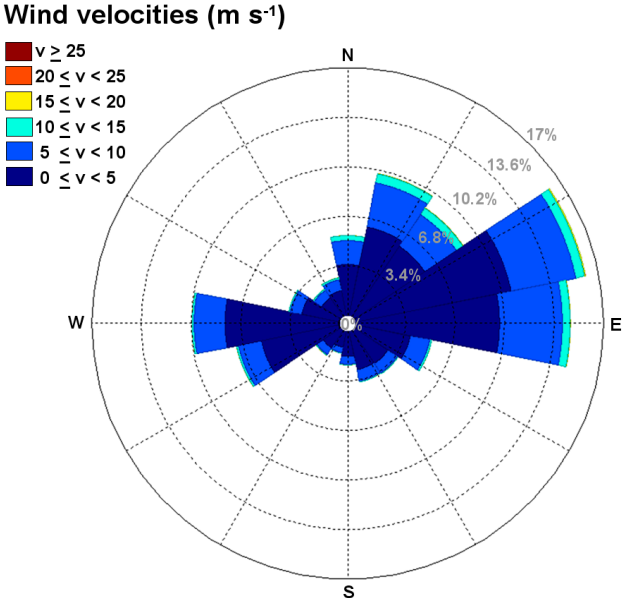

Fig. 2. Wind rose for Qeqertarsuaq from 1995 to 2011 during ice-free months (late May to November; data from the Danish Meteorological Institute 2015).

Methods

Ground-penetrating radar (GPR) data and topographic profiles were measured during a field campaign in August 2015. Elevations, presented as metres above sea level (m a.s.l.), are relative to the chart datum which is the lowest astronomical tide.

Cross-shore profile collection and processing

GPR data were acquired along transects approximately perpendicular to the beach ridges and the present-day beach using shielded 250 MHz transmitter and receiver antennae from Sensors & Software. The antenna configuration and recording settings were similar to those used by e.g. Hede *et al.* (2013) and Nielsen *et al.* (2017). Transmitter and receiver were mounted on a hand-pulled skid plate in contact with the ground. The antennae were placed with a separation of 0.38 m between the antenna centres and in connection with an odometer wheel. We used a recording time window of 450 ns and a trace spacing of 0.05 m; at each recording location eight recordings were stacked into a single trace in order to strengthen the signal-to-noise ratio. Three transects were made across successive beach ridges that lie significantly above present mean sea level, T1,

T2 and T3; seven other transects were obtained close to the present-day beach, two on the sandy beach stretch and five on the coarse-clast beach (Fig. 1C).

The GPR data were processed using the Ekko_Project software package provided by Sensors & Software. The main processing steps were somewhat similar to the ones used by Nielsen & Clemmensen (2009), Hede *et al.* (2013) and Nielsen *et al.* (2017): (1) repositioning of traces, (2) automated 'dewow'-filtering, (3) gain correction using an automatic gain control algorithm with a maximum scaling factor of 200 and window width of 0.5, (4) migration (in some cases) and (5) time-depth conversion and topography correction. Repositioning of traces and topography correction were both based on DGPS measurements acquired with a RTK-Trimble R8 with an accuracy of 0.02 m. These topographic measurements were carried out on the same day as the GPR data collection.

Migration and time-depth conversion are dependent on the radar wave velocity, which is a function of the mean physical material characteristics, water content, and porosity (e.g. Neal 2004). We estimated radar wave velocities based on analysis of diffraction hyperbolas in the recorded un-migrated GPR data. Small variations were observed in both horizontal and vertical directions. Horizontally, wave velocities varied from 0.085 m ns^{-1} below the beach ridges to 0.079 m ns^{-1} below intervening swales. Vertically, wave velocities were higher in the upper parts of the profiles. Hede *et al.* (2013) observed the same, and this velocity decrease with depth is most likely due to increasing water content with depth (Reynolds 1997). For migration and time–depth conversion we used a constant velocity of 0.082 m ns^{-1}, which is the average velocity calculated from vertical and horizontal variations.

The peak frequency of the reflected signals is between 150 and 200 MHz. The vertical resolution is about one fourth of the dominant wavelength (e.g. Jol 1995), which is about 0.1 m in our case. Radar vertical resolution, errors in topographic measurements and interpolation, uncertainties in estimated velocities for time–depth conversion, and possible filtering artefacts account for a total uncertainty of 0.25–0.27 m on the reading of depths based on the GPR data (Nielsen & Clemmensen 2009).

Estimation of significant wave height and wind setup

The significant wave heights (H_s) were estimated using the wind conditions and fetch lengths (Coastal Engineering Research Center 1984). This method only estimates the sea waves whereas swell waves are not included. Wind velocity data from Disko were obtained from the Danish Meteorological Institute (DMI) for the years 1962–1980 and 2000–2014 (DMI 2015). We only used onshore winds from south, south-west and west directions during the ice-free periods.

The maximum potential significant wave heights were verified by an inverse approach using the height of the beach berms (H_b). The run-up level related to H_b is given by the run-up relative to the still-water level (Rsw) plus a high-tide water level. Thus, by measuring the height of beach berms and knowing possible high-tide water levels, we could calculate Rws values. The deep-water significant wave height (H_s) was then estimated using the relationship by Guza & Thornton (1982):

$$Rsw = 0.7\ H_s \qquad \text{(Equation 1)}$$

The wind setup in the embayment was estimated using a simple balance equation (Equation 2) between the force of the wind stress and the pressure gradients that opposed it (Pugh 2004). It assumes steady-state wind conditions, a constant depth of the embayment, and uses a maximum fetch that can generate the highest possible stress (Pugh 2004):

$$S = (C_D\ \rho_A\ W^2)\ /\ (g\ \rho\ D) \qquad \text{(Equation 2)}$$

Where S is the wind setup, C_D is a drag coefficient (*c.* 0.0029), ρ_A is the density of air, W is the wind velocity, g is gravity acceleration, ρ is the density of seawater, and D is water depth.

Results

Only 30% of the winds are from directions favourable for inducing onshore waves during ice-free months at Itilleq. In general, significant wave heights (H_s) are small because the mean wind speed is about 3 m s^{-1}. Winds of 6 m s^{-1}, which is the average speed occurring 21% of the time, should blow for 4 hours over an unlimited fetch to generate a H_s of 0.5 m and a period of 3.3 s and for 10 hours to generate a H_s of 1 m and a period of 5.8 s. Wind speeds above 8.5 m s^{-1} rarely occur, and only one third of such strong winds exceed the average 10.4 m s^{-1} (Fig. 2). Therefore, sea waves are mostly subordinate to tidal water level changes and not dominant at Itilleq. However, swell waves can sometimes occur in Disko Bay.

Table 1 shows the role of the waves for berm formation. Here, we estimated H_s from the heights of berm crests as a function of different tide heights. The estimated H_s are quite high, up to 3.67 m, considering the prevailing mild weather conditions presented above. This means that the berms we observed were built under conditions much more energetic than usual if

tides and waves are the only processes that account for local water level oscillations. However, the wind setup can also play a role. Winds of 10 m s^{-1} over an embayment with a constant depth of 50 m and a maximum fetch length of 100 km give a wind setup of 0.07 m at the beach in our case. However, this contribution does not significantly reduce the estimated H_s value.

Table 1. Significant wave heights (H_s) estimated from run-up heights on sandy beaches at high tide for different berm crest heights and tidal stages. All values in metres.

Profile	BCH	NHT: 1.63 H_s	MHT: 1.81 H_s	SHT: 2.01 H_s
L32	4.20	3.67	3.41	3.13
	3.00	1.96	1.70	1.41
	2.40	1.10	0.84	0.56
L33	4.10	3.53	3.27	2.99
	2.90	1.81	1.56	1.27
	2.00	0.53	0.27	-0.01

BCH: berm crest height. NHT: neap high tide.
MHT: mean high tide. SHT: spring high tide.

Active modern beach geomorphology

Topographic profiles measured along the cross-shore transects on the active sandy beach are about 85 m long and similar in shape, with two distinct berms and a gentle step seaward (Fig. 3A). The gentle steps are at 2 and 2.40 m a.s.l.. Berm crests are at 3 and 4 m a.s.l., which is a height much above the spring high-tide level. The foreshore gradient is 3°.

Cross-shore transects on the coarse-clast beach are shorter, about 35 m long, and the topographic profiles are slightly different from the sandy ones (Fig. 3B). We did not make a systematic analysis of the grain size distribution; however we noted that the size of the clasts on the coarse-clast beach ranged from cobbles (64 to 256 mm in diameter) to boulders (> 256 mm in diameter). Differences in grain size might have caused the moderate differences in the topography between the fine- and coarse-grained beaches. The coarse-clast beach profiles have a step around spring high-tide level and distinct berm crests farther ashore at levels around 3 and 4 m a.s.l.. These observations are similar to what is observed for the sandy beach profiles. However, the gradient of the foreshore is steeper, about 7°. Likewise, the step at around 2 m a.s.l. is more prominent here than for the sandy profiles.

The mean low-tide level is well marked at the modern sandy beach by an abrupt change in sediment size. The foreshore is sandy, while the upper shoreface is characterised by the presence of cobbles and boulders (Fig. 4). Both sediment sizes are expected to be present on the beach and nearshore zone due to the contribution of different local sources (within tens to

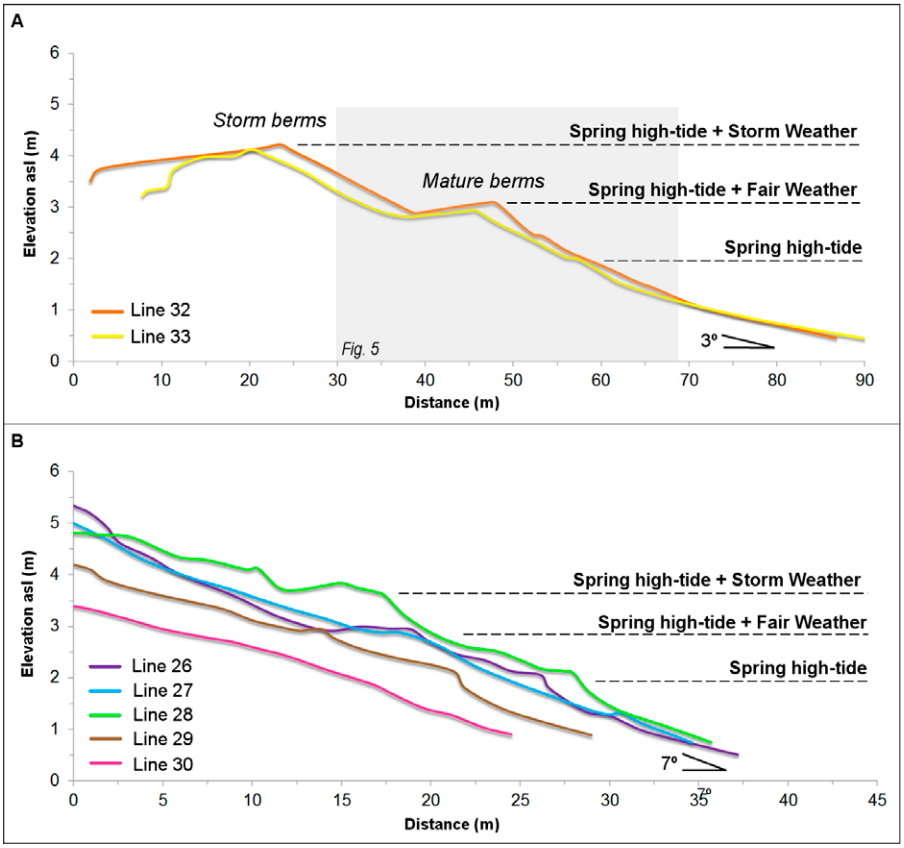

Fig. 3. Active beach topographic profiles. **A**: Profile lines 32 and 33 obtained on the sandy beach. **B**: Profile lines 26 to 30 obtained on the coarse-clast beach. Horizontal dashed lines indicate water levels at various conditions, as labelled. The grey box corresponds to the section shown in Fig. 5. Elevation is related to the chart datum, which is the lowest astronomical tide. Note that the horizontal axes are not at the same scale: profiles in A are twice as long as profiles in B.

Fig. 4. Modern sandy beach at Itilleq. The mean low-tide level is clearly marked by an abrupt change in sediment size: the upper shoreface is characterised by pebbles, cobbles and boulders, while the foreshore is sandy. The red dotted line indicates this sharp transition. The distance between the photographer and the boat was approximately 300 m. Photo August 2015.

hundreds of metres). Fine sediments are likely to be supplied by, for example, the river at the western end of the sandy beach (Fig. 1C). Large clasts are likely to be produced from mountains adjacent to the beach, to be eroded from outcrops by waves during high water levels, and/or to be dragged to the beach by small icebergs and growlers (Nichols 1961).

We interpret the sharp transition around mean low-tide level to be a response to local prevailing fair-weather conditions, when tide oscillation is the process that accounts most for water-level variation. While fine sediment can easily be transported and deposited farther inland to the fore/backshore by swash processes, the larger materials may not. They are unlikely to be remobilised beyond the low water level due to their size and the local prevailing low wave energy. Coastal progradation, however, is an ongoing process and, as it continues, finer material is deposited above the larger clasts, covering the former upper shoreface. The boundary between upper shoreface and foreshore, which corresponds to former mean low-tide levels, is likely to be preserved in the subsurface of the beach deposits (Figs 5 and 6).

Internal sedimentary structures of modern beach deposits

GPR data collected along the beach transects are limited in depth penetration due to salt-water intrusion (Fig. 5). On the sandy beach, we could only image the internal

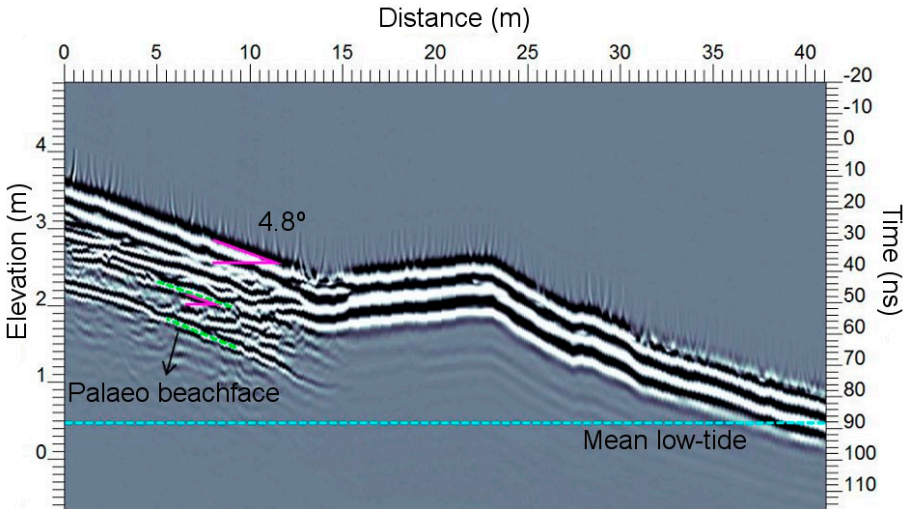

Fig. 5. Migrated GPR reflections from the modern sandy beach (line 32). Green dashed lines exemplify topography-induced radar reflections, interpreted to correspond to palaeo beachface surfaces. Magenta solid lines indicate average slope (4.8°). Low-tide downlap points could not be identified here; they must be at or just below the mean low-tide level (dashed cyan line). Note poor signal penetration presumably due to the conductivity of the salt water in the pores. This profile corresponds to the grey box area in Fig. 3A. Elevation is related to the chart datum, which is the lowest astronomical tide.

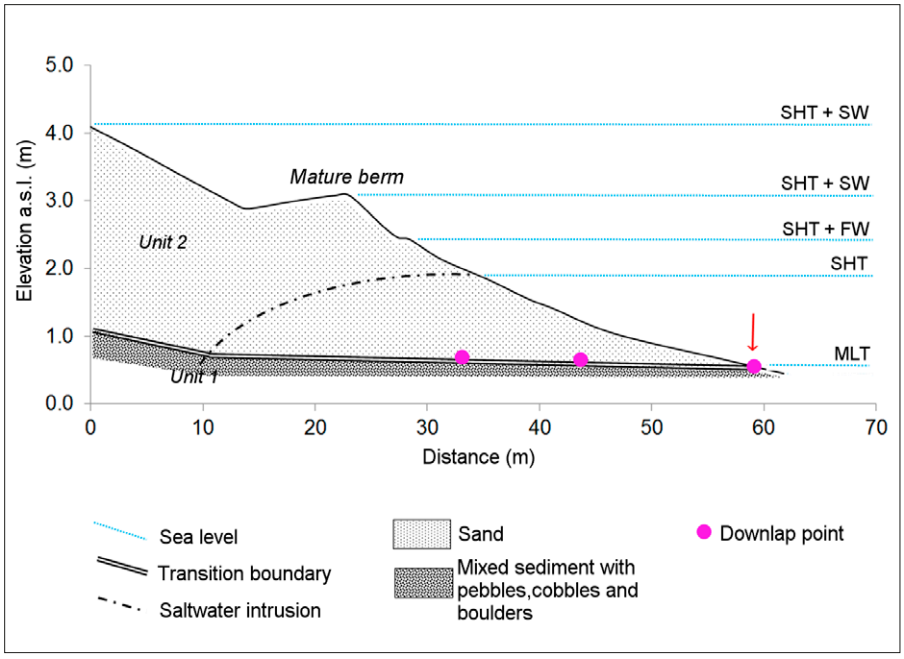

Fig. 6. Observational model of the modern beach at Itilleq based on radar, topographic and visual observations. Horizontal blue lines indicate sea levels determined by: spring high-tide and storm weather with excessive Hs (SHT + SW); spring high-tide and fair weather with low but accountable Hs (SHT + FW); spring high-tide (SHT) and mean low-tide (MLT). Red arrow represents the red dotted line around mean low-tide level in Fig. 4. The model depicts the two sedimentary units we have interpreted, based on GPR data, to correspond to upper shoreface (Unit 1) and foreshore deposits (Unit 2). Unit 1 is characterised by mixed sediment with pebbles, cobbles and boulders, while Unit 2 is sandy. Downlap points (magenta filled circles) occur at the transition boundary, which corresponds to mean low-tide levels. The height of the berm, which eventually becomes a beach ridge, is related to higher sea-water levels. Elevation is related to the chart datum, which is the lowest astronomical tide.

structure of the seaward-dipping flank of the highest berm. All depicted radar reflections lie above mean low-tide level and, similarly to the modern topography, with an average seaward slope of 4.8° (Fig. 5). We therefore interpret these topography-concordant reflections to correspond to palaeo-beachface surfaces. It is expected that these palaeo-beachface reflections are followed downwards by less steep reflections, corresponding to palaeo-shoreface surfaces (Fig. 6). However, since the radar depth penetration was limited to above the mean low-tide level at the modern beach (Fig. 5, dashed blue line), we could not image the upper shoreface regime with GPR at the modern beach. Accordingly, we could not identify downlap points marking the transition between upper shoreface and beachface, but they would presumably be located at or below the mean low-tide level.

Geomorphology of raised, fossil beach ridges

The topography profiles along the GPR transects T1 to T3 show beach ridges and intervening swales (Fig. 7). T1 and T2 both extend from around 40 m a.s.l. near the base of the mountain talus to the coarse-clast beach (Fig. 1C). T1 is 723.80 m long and terminates at the present-day coarse beach. Four zones with different slopes are identified along T1: 6.4° for distances of 0–80 m, 3° for distances of 80–460 m, 1.6° for distances of 460–690 m and 6.3° for distances from 690 m to the end of the transect (Fig. 7A). The slope along T2 varies less, decreasing from *c.* 4.5° at 0–140 m distance to *c.* 3.5° along the remaining profile. Yet there is a noticeable change in the terrain surface of T2 at around 350 m distance because the upper part is quite uneven, with mounds and depressions, whereas the lower part is much more even (Fig. 7B). T3 is shorter and does not cover the oldest successive raised beach ridges (Fig. 1C). The slope is not steep (*c.* 4°), yet it becomes *c.* 2° flatter from 100 to 180 m distance (Fig. 7C).

In general, the observed changes in the terrain slope along transects T1 and T3 follow changes in the sedimentary structure of the beach ridges from 0 to *c.* 1 m below the surface: the slope is less steep where fine-grained sediments are more abundant (Figs 7, 8A–B and 8D–F). An exception is observed in T1 for profile distances 638–738 m (Fig. 7A), where coarse clasts (>64 mm in diameter) are dominant over fine sediment, yet the slope is not steep (Fig. 8C).

Internal sedimentary structures of fossil beach deposits

The applied radar antennae and the characteristics of the sediment allowed us to image the raised beaches to depths of about 3 m below the surface (Fig. 9). The very top part was affected by arrival of the direct air wave. Below this arrival, we identified two radar units separated by a clear boundary at about 1.5 m below the surface and approximately parallel to the overall topography (Fig. 10A). From here on, this boundary will be referred to as the transition boundary. In general, caution must be taken regarding interpretation of

arrivals from below this transition boundary. Reflections below the transition boundary are weak and may be affected by multiple arrivals from shallower levels. Marked diffractions (observed as hyperbolas in unmigrated GPR sections) originating from the transition boundary characterise several intervals of the GPR sections (Fig. 10A). The unit above the transition boundary (Unit 2) is characterised by subparallel, continuous reflections dipping seaward by 0.5° to 2° (Fig. 10A). This pattern is present along most of the profiles, but exceptions occur, mainly beneath swales, where the transition boundary is not as evident due to fuzzier reflections. Here, the diffractions from the top of the lower unit (Unit 1) appear relatively stronger in comparison to those observed beneath the ridges (Fig. 10A, for example).

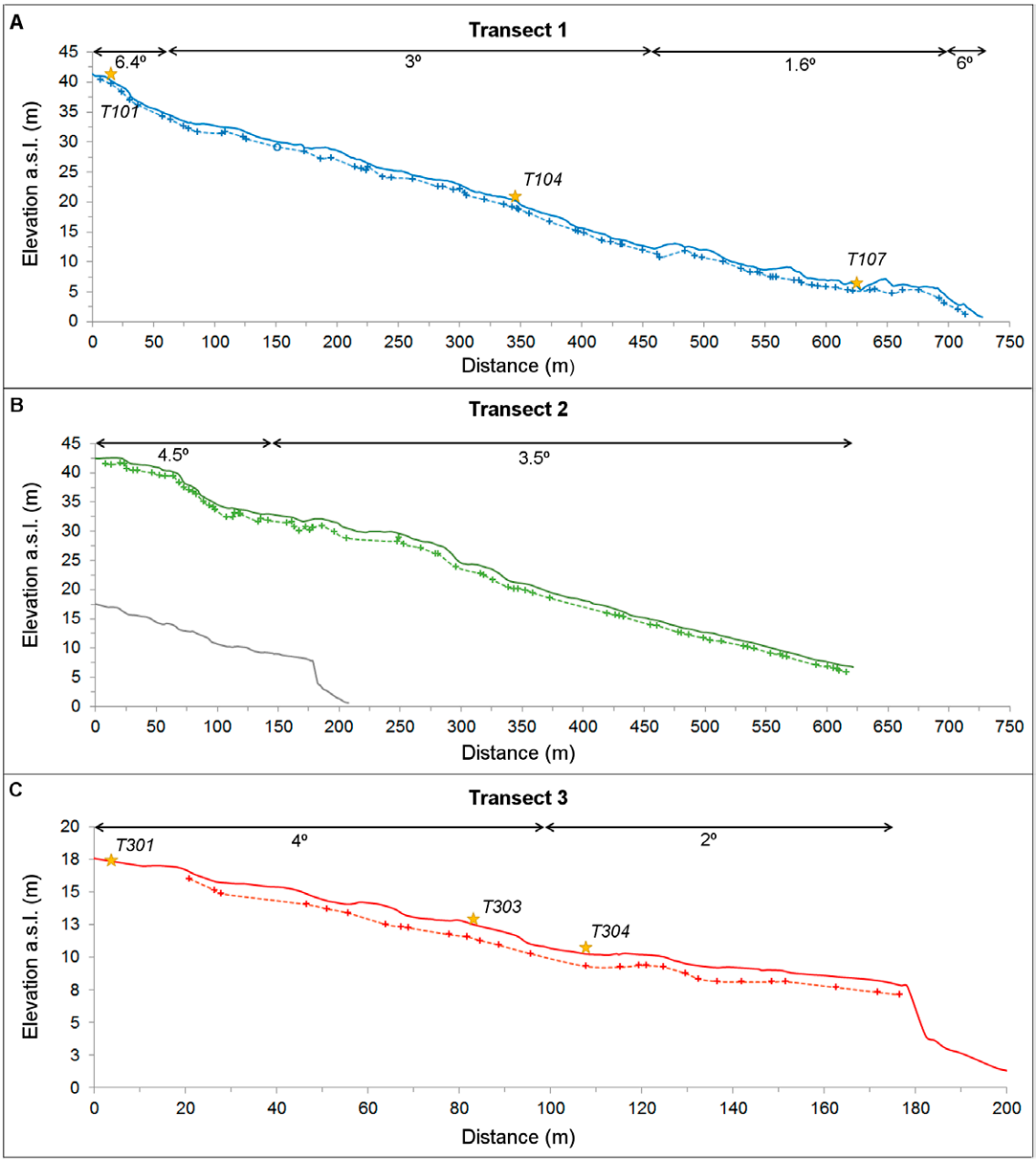

Fig. 7. Transect profiles across successive raised beach ridges. Continuous lines correspond to differential GPS measurements; dashed lines are constructed from the elevation of individual downlap points (crosses along the dashed line) identified in the GPR images; yellow stars show the location of holes; horizontal arrows indicate the extent of stretches of similar topographic slopes. Note that the vertical and horizontal scales in C are different from those in A and B because Transect 3 is considerably smaller than the other two transects. For comparison, Transect 3 is plotted in grey below Transect 2 in B. Elevation is related to the chart datum, which is the lowest astronomical tide.

Two types of seaward-dipping sets of downlap points were identified: one occurring within Unit 2 at shallow levels between 0.5–1.5 m below the surface (Fig. 10B, green circles) and one at a slightly deeper level. We only identified a few of the shallow downlap points. We interpret these shallow downlap points to correspond to the transition between foreshore and upper shoreface at higher sea levels at the time of deposition of storm berms.

A set of deeper downlap points marks the transition boundary (Fig. 10B, magenta circles). They are frequently present along all profiles. We interpret the deeper downlap points as corresponding to the mean low-tide level at the time of deposition, consistent with Nielsen *et al.* (2017). The points mark the transition to a deep layer with strong signal scattering (Fig. 10), which most likely was produced by an abrupt change in sediment properties such as a clast-size increase downwards. This sharp lithological boundary resembles what we have observed around mean low-tide level (Fig. 4) during fair weather conditions on the present active sandy beach (Fig. 1C).

The locations of these GPR markers of palaeo mean low-tide level are shown in Fig. 7 (crosses along dashed lines). The highest downlap points identified along T1 and T2 indicate a relative sea level of about 40 m above the present sea level (Fig. 7A).

Discussion

Mature berms under calmer conditions are often correlated to high-tide levels or to mean water levels in case of non-tidal environments (Bendixen *et al.* 2013). Itilleq represents a micro- to meso-tidal environment and the mature modern berm height at 3 m a.s.l. is well above the high-tide levels (Fig. 3A). This suggests that other processes, besides the prevailing high-tide levels, must have contributed to produce the higher sea levels at which berm crests were deposited. Therefore, berm crest height cannot be directly related to mean sea level at the time of deposition at Itilleq.

The upper shoreface and foreshore deposits on

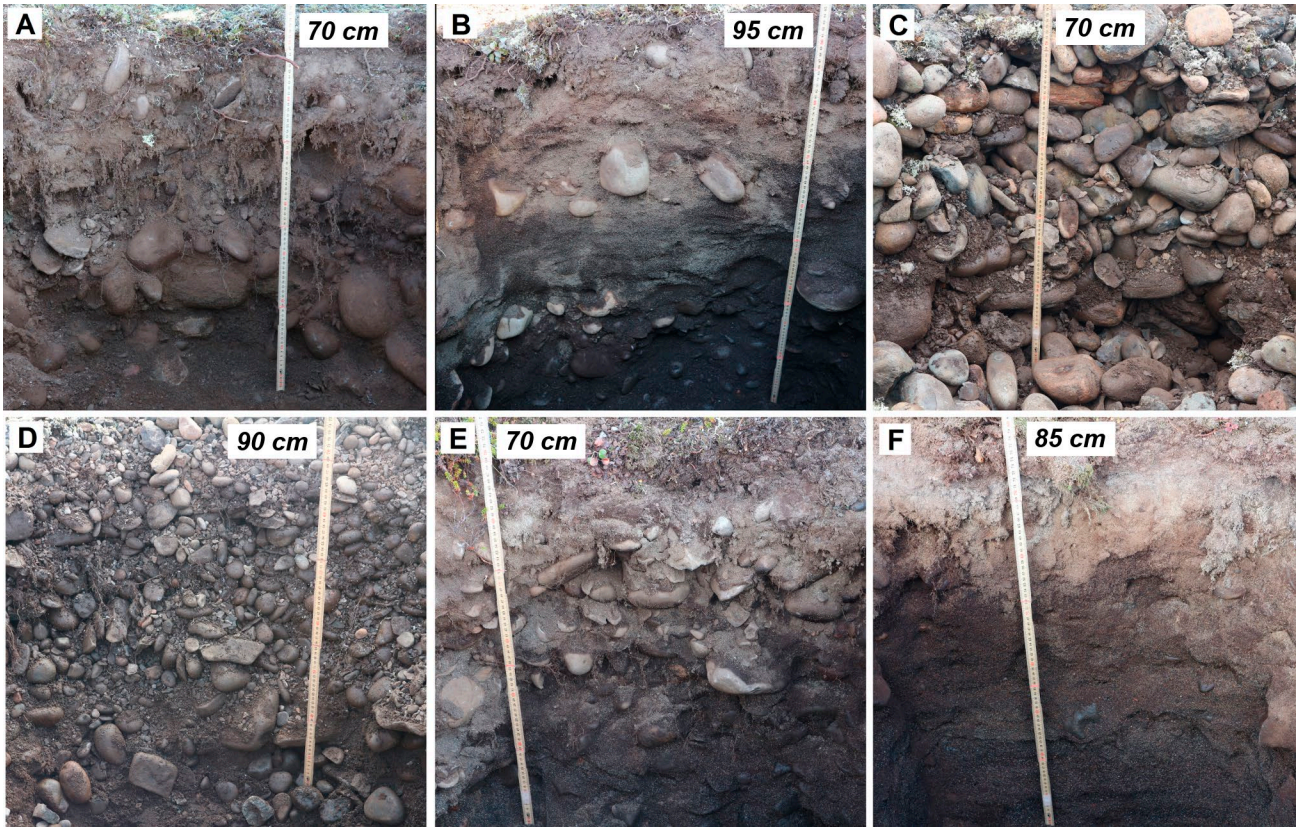

Fig. 8. Photographs of holes dug along transects T1 (A, B and C) and T3 (D, E and F). **A**: Hole T101 was 70 cm deep and located on the oldest beach ridge covered by GPR measurements (*c.* 40 m a.s.l.). **B**: Hole T104 was 95 cm deep and located in the central part of T1 (*c.* 20 m a.s.l.). **C**: Hole T107 was 70 cm deep and located at the end of T1 (*c.* 6 m a.s.l.), close to the present-day coarse-clast beach. **D**: Hole T301 was 90 cm deep and located at the oldest beach ridge of T3 (*c.* 16 m a.s.l.). **E**: Hole T303 was 70 cm deep and located in the central part of T3 (*c.* 12 m a.s.l.). **F**: Hole T304 was 85 cm deep and located about 30 m from T303, at *c.* 10 m a.s.l..

the present-day beach, however, are well defined, as seen for several other prograding beach deposits (e.g. Tamura *et al.* 2008; Nielsen & Clemmensen 2009; Clemmensen & Nielsen 2010; Billy *et al.* 2015; Nielsen *et al.* 2017). At Itilleq the boundary between them is observed as an abrupt change in sediment grain size and appears to coincide approximately with the mean low-tide level (Fig. 4). This boundary is likely to be preserved and delineated by downlap points in the internal sedimentary architecture of raised beach deposits (Fig. 6). Similarly, Tamura *et al.* (2008) have shown that the boundary between upper shoreface and foreshore facies on a beach plain in Japan corresponds to about 1 m below mean sea level, which is the local spring low-tide level. Nielsen & Clemmensen (2009) have shown that the downlap points identified on GPR reflections from a modern beach of the micro-tidal regime in the Kattegat Sea correspond to the mean sea-level at the time of deposition.

The transition between foreshore and upper shoreface deposits is often observed by a marked change in the bed morphology on radar profiles. Foreshore deposit reflections are moderately continuous, gently seaward-dipping, and followed vertically downwards by more complex reflections, which characterise upper shoreface deposits (Tamura *et al.* 2008; Nielsen & Clemmensen 2009; Clemmensen & Nielsen 2010; Nielsen *et al.* 2017). In this study, while foreshore reflections are noticeable and of characteristic bed shape along the T1, T2 and T3 transects, typical upper shoreface cross-bedding reflections cannot be clearly identified due to diffractions and a relatively week signal-to-noise ratio (Fig. 9). Nevertheless, GPR signal scattering is consistent with the abrupt change of sediment grain size observed around mean low-tide level on the modern beach. Such consistency supports the interpretation that the lower GPR unit corresponds to palaeo upper shoreface deposits.

Permafrost is known to cause reflectivity in GPR data sections (e.g. Jørgensen & Andreasen 2006). We cannot rule out that permafrost may contribute to some of the reflectivity observed in our GPR reflection sec-

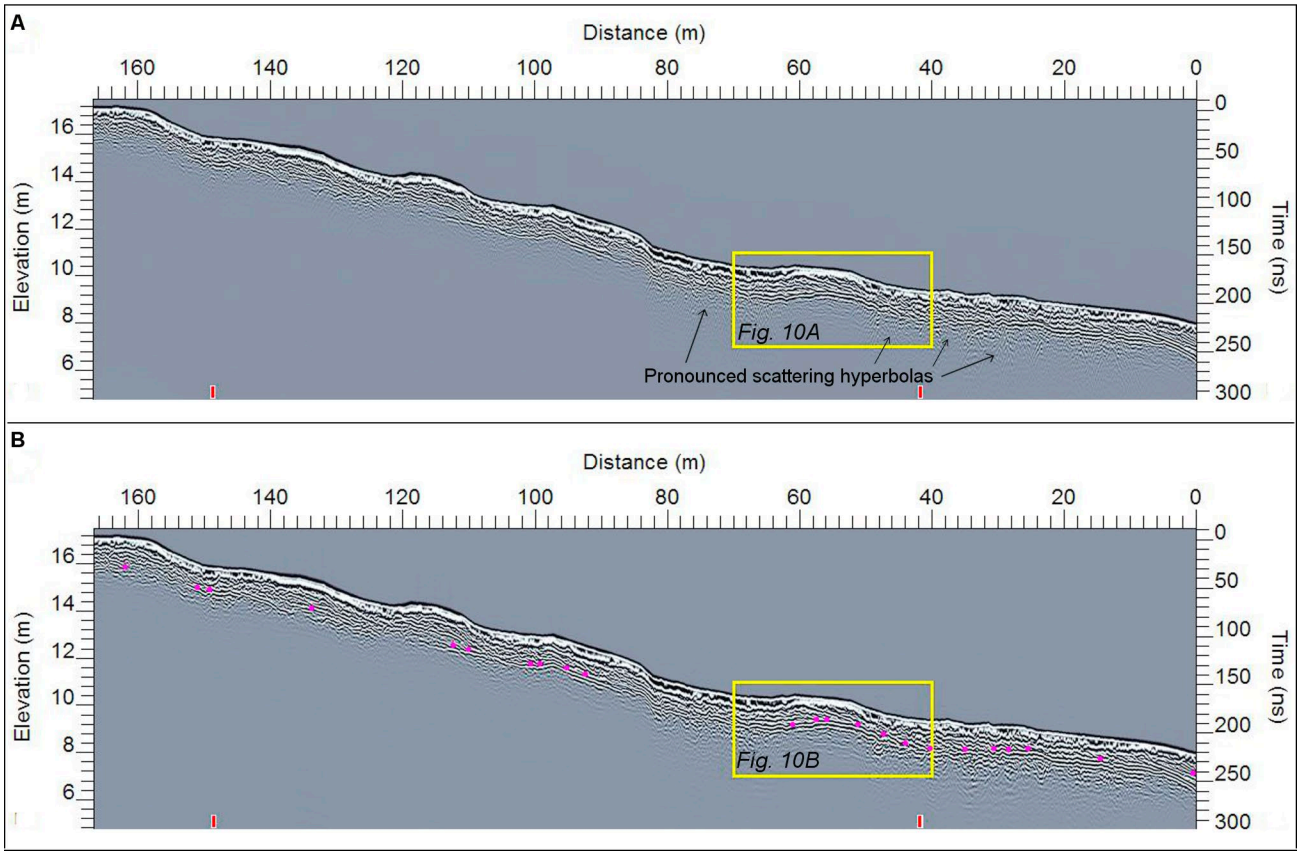

Fig. 9. GPR reflections from Transect T3. **A**: Non-migrated data: scattering hyperbolas are present around 1.5 m below terrain surface all over the radar profile, but they are stronger and more frequent in some places (indicated by arrows). **B**: Migrated data: pink dots show some downlap points identified along T3, which are the same as plotted along the dashed line in Fig. 7C. Yellow boxes in both A and B correspond to the section shown in greater detail in Figs 10A and B. Note that the horizontal axis is in reverse direction compared to Fig. 9; this is because the GPR data of Transect 3 was collected from the youngest (and lowest) towards the oldest beach ridges. Elevation is related to the chart datum, which is the lowest astronomical tide.

tion, e.g. where the transition from the upper unit to the lower unit appears as a relatively strong reflection. However, permafrost was not encountered in any of the holes up to *c.* 1 m deep that were dug for our study. Besides, we would expect to find permafrost below the swales due to ice grown in soils with high water content, and not below the beach ridges.

Gravelly beach ridges are expected to be formed under energetic wave conditions (Otvos 2000). However, if the local source of coarse-grained sediment is very close, the shoreline consists of gravelly berms, and consequently gravelly beach ridges. Sources of large clasts (mountain and eroding outcrop, see Fig. 1C) are within only tens to hundreds of metres from the beach at Itilleq, and swash and backwash processes can easily build the beach ridges. Growlers (fragmented ice) could also contribute by dragging clasts of various sizes, including large boulders (Nichols 1961). Large cobbles and boulders, however, are likely to be restricted to the upper shoreface because they cannot be easily reworked by swash processes once they settle on the beach.

Changes in the sedimentary structure of successive beach ridges suggest different local sediment sources. From T101 to T104 (Fig. 8A and B), for example, large clasts become less abundant and more diverse (with regard to mineralogy) in the sedimentary matrix as the beach ridges are situated farther from the inland mountain (see Fig.1C for location). Clasts in T101 are likely to be derived from the adjacent basaltic mountain, while clasts in T104 could be delivered from the mountain but also from other sources, i.e. they could be non-basaltic ice-transported material (see light-coloured rocks in Fig. 8B). Besides, fine sediment is abundant in the sedimentary matrix of T104, which implies that another source besides the mountain has become important. Another change in the main sediment source has probably taken place between T104 and T107. Unlike T104, the sedimentary matrix of T107 is coarse-grained and supports clasts larger than 10 cm in diameter, and almost devoid of sand (Fig. 8C). In fact, it resembles the present-day coarse-clast beach, which is *c.* 200 m distant (Fig. 1C). It may be

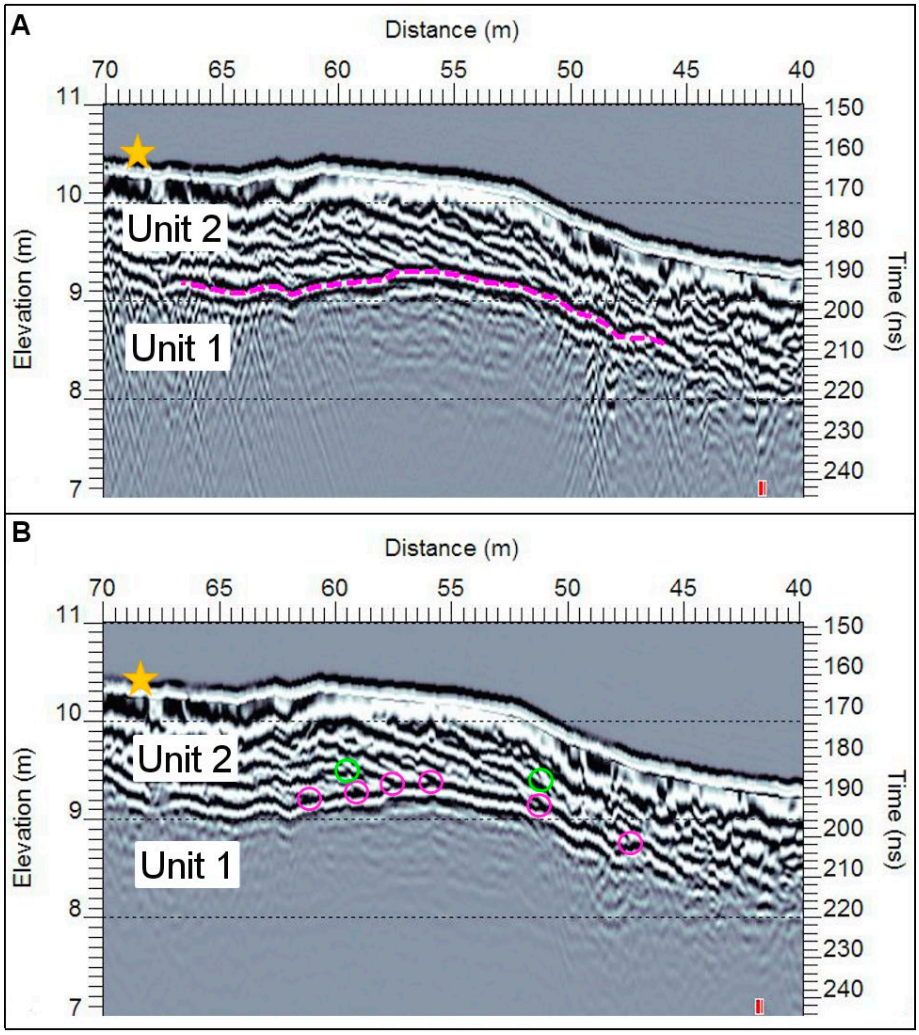

Fig. 10. Section of GPR reflections from Transect T3 at distances 70 to 40 m (yellow boxes in Fig. 9). **A**: Non-migrated radar image showing the transition boundary (dashed magenta line) between units 1 and 2. **B:** Migrated radar image showing some downlap points identified at the transition boundary (magenta circles) or just above it (green circles), within Unit 2. See text for interpretation. Yellow star shows the location of Hole T304. Elevation is related to the chart datum, which is the lowest astronomical tide.

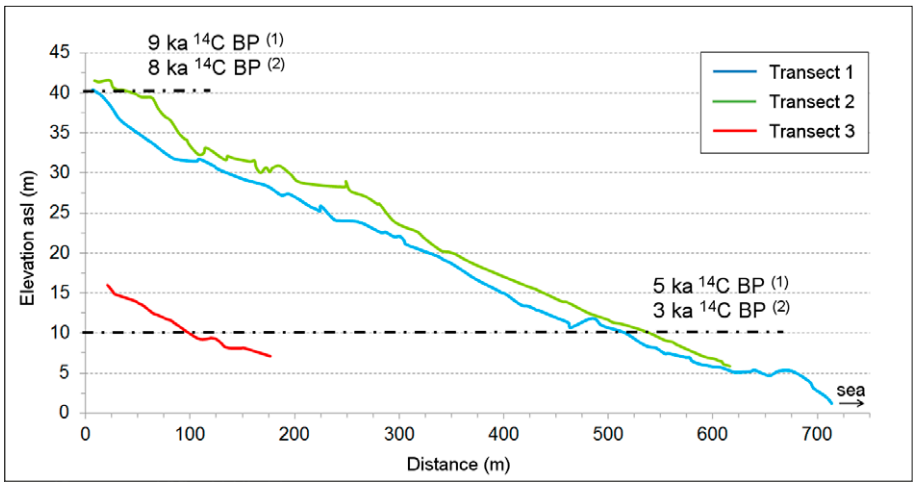

Fig. 11. First order age model for palaeo-sea levels at Itilleq. Transect profiles are based on the elevation of downlap points, which represent palaeo mean low-tide levels. Dash-dotted black lines show the elevation of palaeo-sea levels radiocarbon dated by Ingólfsson *et al.* 1990 (1) and Rasch & Nielsen 1995 (2) at 40 and 10 m a.s.l.. Elevation is related to the chart datum, which is the lowest astronomical tide.

that the same sediment source has contributed to their formation.

The sedimentary matrix of the beach ridges also varies along T3, showing a decrease in sediment grain size from the higher to the lower parts of the transect (Fig. 8D-F). T301 resembles T107, with clasts of various sizes and apparently of different mineralogy (see clasts of various colours in Fig. 8D). As in T107, the clasts here could have originated from eroding outcrops. At T303 finer sediments (sand) are as abundant as large clasts (Fig. 8E), and at T304 the sedimentary matrix is mainly sandy and almost devoid of large clasts (Fig. 8F). Again, we can infer a change in the role of local sediment sources over time. Here, the river at the western end of the sandy beach is likely to be the major source of sand (Fig. 1C).

We have observed changes in the sedimentary matrix down to 70 to 95 cm depth (Fig. 8). In some parts of the profiles we observe relatively strong GPR scattering hyperbolas at the level (*c.* 1.5 m below the surface) which we interpret to represent the top of the upper shoreface palaeo deposits (for example, Fig. 10A at distances 67–70 m and 51–40 m). We assume that the strong diffractions indicate the existence of relatively large clasts. The fact that they do not occur at this level all through the profiles suggests, again, changes in the role of the main sediment source.

Optically Stimulated Luminescence (OSL) dating is commonly used for dating sedimentary deposits without material suitable for ^{14}C-dating (Murray & Olley 2002; Pedersen *et al.* 2011). However, it is difficult to apply standard OSL techniques at our field site because of the very limited amount of sand fraction material in the matrix. Therefore, we used existing curves based on radiocarbon dates from the broader Disko Bay area to provide a first order age model for the late Holocene at Itilleq. Datings made by Ingólfsson *et al.* (1990) suggest ages of 9 ka ^{14}C BP and 5 ka ^{14}C BP for palaeo-sea levels at 40 and 10 m a.s.l., respectively (Fig. 11). Datings by Rasch & Nielsen (1995) suggest slightly younger ages for the same palaeo-sea levels: 8 ka ^{14}C BP at 40 m a.s.l. and 3 ka ^{14}C BP at 10 m a.s.l. (Fig. 11). Roughly, these intervals represent an overall relative sea-level fall rate of 0.6–0.7 cm a^{-1} from 9 ka ago to present day.

Conclusions

At Itilleq, berms are deposited above the sea level reached during high tides. They are most likely deposited under sporadically occurring high-energy conditions, and their height does not reflect mean sea level.

On the sandy beach, the mean low-tide level is well defined by an abrupt change in sediment grain-size: the foreshore is characterised by sand, whereas the upper shoreface is characterised by coarse clasts. As beach progradation continues, upper shoreface coarse deposits are overlain by foreshore sediment, and the boundary between them is preserved in the fossil beach deposits.

Sources of both fine and coarse sediments are likely to be both local and ice-transported. However, differences in grain size and mineralogy of sedimentary structures along the transects suggest that different sources have played variable roles over time.

We identified several seaward-dipping downlap points in the GPR reflection data collected over the raised beach ridges at Itilleq. Most of these downlap points are located at the transition boundary between two radar units with different reflection patterns. Diffractions characterise the transition from upper shoreface to foreshore deposits in many places. Based on our observations on the modern active beach, we interpret the diffractions to be caused by an abrupt change (increase) in sediment size. Consequently, the downlap points located at the transition boundary can be used as proxies for past mean low-tide levels.

Acknowledgements

We acknowledge funding by Geocenter Denmark, the Brazilian Government's program Science Without Borders (CNPq), and Independent Research Fund Denmark. We thank Sigurd Bohr, Asger Meldgaard and Bruno Bainy for their contributions during field work in 2016. Further, we thank Ingelise Møller Balling, Gunver Krarup Pedersen, Michael Houmark-Nielsen, and Lotte Melchior Larsen for their comments on an earlier version of this manuscript, which greatly helped improve the manuscript.

References

Bendixen, M., Clemmensen, L. & Kroon, A. 2013: Sandy berm and beach-ridge formation in relation to extreme sea-levels: a Danish example in a micro-tidal environment. Marine Geology 344, 53–64.

Billy, J., Robin, N., Hein, C.J., Certain, R. & FitzGerald, D.M. 2015: Insight into the late Holocene sea-level changes in the NW Atlantic from a paraglacial beach-ridge plain south of Newfoundland. Geomorphology 248, 134–146.

Coastal Engineering Research Center (CERC) 1984: Shore protection manual (4th edition), Chapter 3: Wave and water level predictions, 143 pp. Vicksburg: Coastal Engineering Research Center.

Clemmensen, L.B. & Nielsen, L. 2010: Internal architecture of a raised beach system (Anholt, Denmark) resolved by ground-penetrating radar investigations. Sedimentary Geology 223, 281–290.

Danish Meteorological Institute (DMI) 2015: http://www.dmi.dk/en/groenland/ [29 September 2015].

Donner, J. 1978: Holocene history of the west coast of Disko, Central West Greenland. Geografiska Annaler 60, 63–72.

French, H. 1996: The periglacial environment, 341 pp. Harlow: Longman.

Guza, R. & Thornton, E. 1982: Swash oscillations on a natural beach. Journal of Geophysical Research 87, 483–491.

Hede, M.U., Bendixen, M., Clemmensen, L.B., Kroon, A. & Nielsen, L. 2013: Joint interpretation of beach-ridge architecture and coastal topography show the validity of sea-level markers observed in ground-penetrating radar data. The Holocene 23(9), 1238–1246.

Ingólfsson, Ó., Povl, F., Funder, S. & Humlum, O. 1990: Palaeoclimatic implications of an early Holocene glacier advance on Disko Island, West Greenland. Boreas 19, 297–311.

Jol, H.M. 1995: Ground penetrating antennae frequencies and transmitter powers compared for penetration depth, resolution and reflection continuity. Geophysical Prospecting 43, 693–709.

Jørgensen, A.S. & Andreasen, F. 2007: Mapping of permafrost surface using ground-penetrating radar at Kangerlussuaq Airport, western Greenland. Cold Regions Science and Technology 48, 64–72.

Lindhorst, S. & Shutter, I. 2014: Polar gravel beach-ridge systems: Sedimentary architecture, genesis, and implications for climate reconstructions (South Shetland Islands/Western Antarctic Peninsula). Geomorphology 221, 187–203.

Murray, A.S. & Olley, J.M. 2002: Precision and accuracy in the optically stimulated luminescence dating of sedimentary quartz: a status review. Geochronometria 21, 1–16.

Neal, A. 2004: Ground-penetrating radar and its use in sedimentology: principles, problems and progress. Earth-Science Reviews 66, 261–330.

Nichols, R.L. 1961: Characteristics of beaches formed in polar climates. American Journal of Science 259, 694–708.

Nielsen. L. & Clemmensen, L.B. 2009: Sea-level markers identified in ground-penetrating radar data collected across a modern beach ridge system in a microtidal regime. Terra Nova 21, 474–479.

Nielsen, L., Bendixen, M., Kroon, A., Hede, M., Clemmensen, L., Weβling, R. & Elberling, B. 2017: Sea-level proxies in Holocene raised beach ridge deposits (Greenland) revealed by ground-penetrating radar. Scientific Reports 7, Article number 46460. doi:10.1038/srep46460.

Otvos, E.G. 2000: Beach ridges - definition and significance. Geomorphology 32, 83–108.

Pedersen, A.K., Ulff-Møller, F., Larsen, L.M., Pedersen, G.K. & Dueholm, K.S. 2000: Geological Map of Greenland, 1:100 000, Uiffaq 69 V.1 Syd. Copenhagen: Geological Survey of Denmark and Greenland.

Pedersen, J.B.T., Kroon, A. & Jakobsen, B.H. 2011: Holocene sea-level reconstruction in the Young Sound region, Northeast Greenland. Journal of Quaternary Science 26, 219–226.

Pugh, D. 2004: Changing Sea-levels: Effects of Tides, Weather and Climate, 265 pp. Cambridge: Cambridge University Press.

Rasch, M. & Nielsen, N. 1995: Coastal morpho-stratigraphy and Holocene relative sea-level changes at Tuapaat, southeastern Disko Island, central West Greenland. Polar Research 14, 277–289.

Reynolds, J. 1997: An Introduction to Applied Environmental Geophysics, 806 pp. Chichester: Wiley.

Rodriguez, A. & Meyer, C. 2006: Sea-level variation during the Holocene deduced from the morphologic and stratigraphic evolution of Morgan Peninsula, Alabama, U.S.A.. Journal of Sedimentary Research 76, 257–269.

Simms, A.R., DeWitt, R., Kouremenos, P. & Drewry, A. 2011: A new approach to reconstructing sea levels in Antarctica using optically stimulated luminescence of cobble surfaces. Quaternary Geochronology 6, 50–60.

Tamura, T., Murakami, F., Nanayama, F., Watanabe, K. & Saito, Y. 2008: Ground-penetrating radar profiles of Holocene raised-beach deposits in the Kujukuri strand plain, Pacific coast of eastern Japan. Marine Geology 248, 11–27.